

RESEARCH ARTICLE

10.1029/2018JB017211

Special Section:

Creep on Continental Faults and Subduction Zones: Geophysics, Geology, and Mechanics

Key Points:

- 2,313 earthquakes located in the Hikurangi margin, using ocean bottom seismometers and absolute pressure gauges from a temporary experiment
- Abundant earthquakes in the subducting Pacific plate suggest bending stress-related fractures allowing upward migration of fluids
- Microseismic gap identified at down-dip limit of the September–October 2014 slow slip event coincides with interseismic coupling

Supporting Information:

- Supporting Information S1
- Table S1

Correspondence to:

J. Yarce,
jefferson.yarce@colorado.edu

Citation:

Yarce, J., Sheehan, A. F., Nakai, J. S., Schwartz, S. Y., Mochizuki, K., Savage, M. K., et al. (2019). Seismicity at the northern Hikurangi Margin, New Zealand, and investigation of the potential spatial and temporal relationships with a shallow slow slip event. *Journal of Geophysical Research: Solid Earth*, 124, 4751–4766. <https://doi.org/10.1029/2018JB017211>













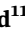

Received 18 DEC 2018

Accepted 6 APR 2019

Accepted article online 10 APR 2019

Published online 13 MAY 2019

Seismicity at the Northern Hikurangi Margin, New Zealand, and Investigation of the Potential Spatial and Temporal Relationships With a Shallow Slow Slip Event

J. Yarce^{1,2} , A. F. Sheehan^{1,2} , J. S. Nakai^{1,2} , S. Y. Schwartz³ , K. Mochizuki⁴ , M. K. Savage⁵ , L. M. Wallace^{6,7} , S. A. Henrys⁷ , S. C. Webb⁸ , Y. Ito⁹ , R. E. Abercrombie¹⁰ , B. Fry⁷ , H. Shaddox³ , and E. K. Todd¹¹ 

¹Department of Geological Sciences, University of Colorado Boulder, Boulder, CO, USA, ²Cooperative Institute for Research in Environmental Sciences (CIRES), University of Colorado Boulder, Boulder, CO, USA, ³Department of Earth and Planetary Sciences, University of California, Santa Cruz, California, USA, ⁴Earthquake Research Institute, University of Tokyo, Tokyo, Japan, ⁵Institute of Geophysics, School of Geography, Environment and Earth Sciences, Victoria University of Wellington, Wellington, New Zealand, ⁶Institute for Geophysics, University of Texas at Austin, Austin, TX, USA, ⁷GNS Science, Lower Hutt, New Zealand, ⁸Lamont-Doherty Earth Observatory, Columbia University, New York, NY, USA, ⁹Disaster Prevention Research Institute, Kyoto University, Kyoto, Japan, ¹⁰Department of Earth and Environment, Boston University, Boston, MA, USA, ¹¹Department of Geology, University of Otago, Dunedin, New Zealand

Abstract In 2014–2015, the Hikurangi Ocean Bottom Investigation of Tremor and Slow Slip experiment deployed seafloor absolute pressure gauges and ocean bottom seismometers directly above a large slow slip event, allowing examination of the relationship between slow slip and earthquakes in detail. Hikurangi Ocean Bottom Investigation of Tremor and Slow Slip data were combined with nearby existing land stations to create a catalog of microseismicity consisting of 2,300 earthquakes ranging in magnitude between 0.5 and 4.7 that is complete to magnitude 1.5, yielding almost twice as many events as detected by the onshore networks alone. This greatly improves the seismicity catalog for this active subduction zone margin, especially in the offshore portion that was difficult to study using only the inland permanent seismic network. The new locations for the events within the footprint of the offshore network show that earthquakes near the trench are systematically shallower than and NW (landward) of their locations using only land-based stations. Our results indicate that Hikurangi seismicity is concentrated in two NE–SW bands, one offshore beneath the outer forearc wedge, one onshore beneath the eastern Raukumara Peninsula, and the majority of earthquakes are within the subducting Pacific plate with a smaller percent at the plate interface. We find a 20-km wide northeast trending gap in microseismicity between the two bands and beneath the inner forearc wedge and this gap in seismicity borders the downdip edge of a slow slip patch.

1. Introduction

The Hikurangi margin is an active subduction zone located off the east coast of New Zealand's North Island, where the Pacific Plate subducts beneath the eastern North Island (Australian Plate; Figure 1). The Pacific Plate converges with the eastern North Island along the Hikurangi trough at a rate of 50–60 mm/year in the northernmost section of the margin, decreasing to approximately 20 mm/year at the southern section (Wallace et al., 2004). This margin has experienced large magnitude earthquakes, some accompanied by tsunamis, and tens of slow slip events (SSEs). Two tsunami earthquakes (Kanamori, 1972) occurred near the North Island's east coast offshore of Poverty Bay and Tokomaru Bay in 1947 (Bell et al., 2014; Doser & Webb, 2003; Figure S1 in the supporting information). Both seismic events had moment magnitudes of ~7.0 and generated tsunamis with wave heights greater than 6 and 10 m, respectively (Doser & Webb, 2003). A more recent normal faulting intraslab event (M_W 6.7 at 24-km depth) occurred in December 2007 offshore Gisborne (François-Holden et al., 2008), and several buildings were significantly damaged, three of which collapsed.

Over the last two decades, the Hikurangi margin has been the focus of extensive research investigating SSEs. SSEs involve transient slip lasting from days to months—at a rate much slower than earthquakes and much

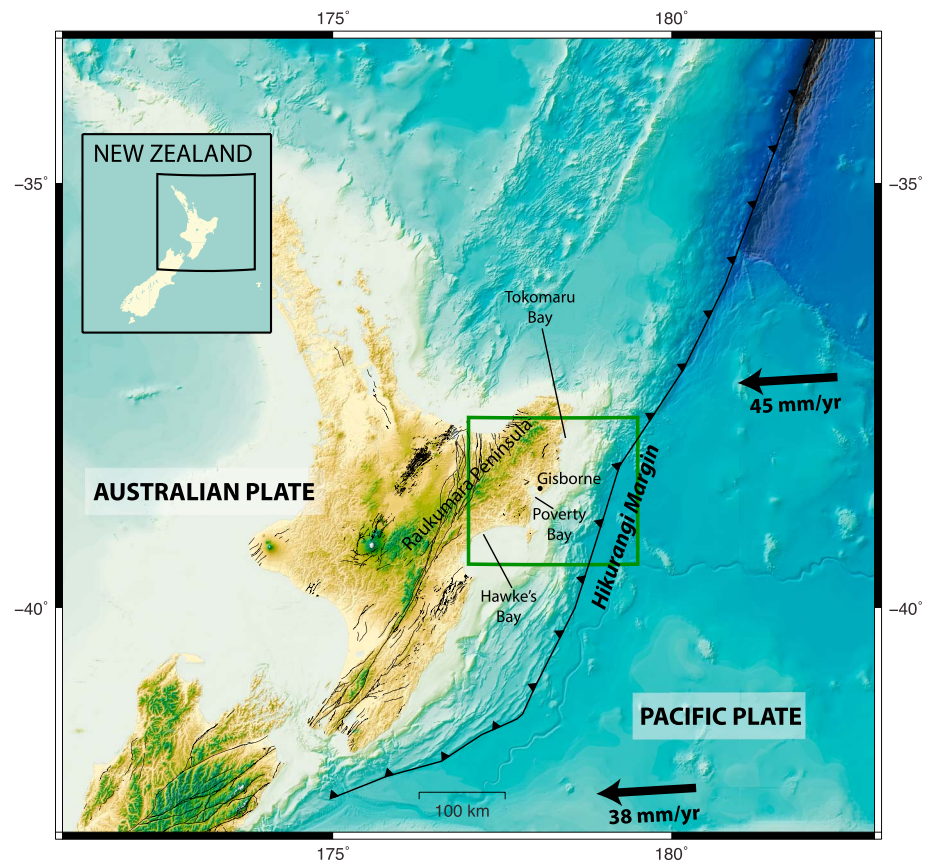


Figure 1. Tectonic setting of the Australian-Pacific plate boundary. Green square indicates the location of the Hikurangi margin and HOBITSS experiment. Black thick lines indicate the approximate location of the plate tectonic boundaries, and thin black lines are the active faults on New Zealand (Langridge et al., 2016).

faster than typical tectonic plate motions. The SSEs of the northern Hikurangi margin near Gisborne, New Zealand, occur at very shallow depths (<15 km). Previous studies of these Hikurangi SSEs have investigated slip distribution determined using Global Positioning System (GPS) and modeling (Bartlow et al., 2014; Douglas et al., 2005; McCaffrey, 2014; McCaffrey et al., 2008; Wallace et al., 2016, 2017, 2018; Wallace, Beavan, et al., 2012; Wallace & Beavan, 2010; Wallace & Eberhart-Phillips, 2013), detection and location of tectonic tremor (Kim et al., 2011; Todd et al., 2018; Todd & Schwartz, 2016), analysis of the relation of SSEs to slab and interface seismicity (Jacobs et al., 2016; Warren-Smith, Fry, Kaneko, et al., 2018), and detailed seismic imaging (Barker et al., 2009; Bell et al., 2010). SSEs have been observed to occur in the northern Hikurangi margin approximately every 18 to 24 months (Wallace & Beavan, 2010). From 2002 to the present, dozens of SSEs at the Hikurangi margin have been detected (Wallace et al., 2017; Wallace & Beavan, 2010; Wallace & Eberhart-Phillips, 2013). The best recorded episode of slow slip with moment release equivalent to a magnitude M_W 6.8 earthquake was observed in September–October 2014 during the Hikurangi Ocean Bottom Investigation of Tremor and Slow Slip (HOBITSS) deployment. Combining land-based continuous GPS stations together with vertical displacements from absolute pressure gauges (APGs), it was determined that this event lasted for approximately 2–3 weeks, had an estimated maximum slip of >20 cm at a depth of approximately 9 km on the interface, and produced vertical displacement of up to 5.4 cm (Wallace et al., 2016).

These quasiperiodic SSEs have been detected in many subduction systems, most of them occurring in the circum-Pacific Rim including Japan, Cascadia (northwestern United States), Costa Rica, southern Mexico, Alaska, and New Zealand's North Island (Peng & Gomberg, 2010; Schwartz & Rokosky, 2007; Figure 1). In many cases, SSEs can be associated with elevated rates of seismicity (Delahaye et al., 2009; Vallée et al., 2013), including moderate magnitude ($M_w \sim 5$ –6; Wallace et al., 2017) or even higher magnitude earthquakes such as the 2011 Tohoku megathrust event (M_w 9.0–9.1; Uchida et al., 2016). Many hypotheses have been

suggested to explain the physical mechanisms that lead to transient slow slip behavior, but there is not yet a consensus opinion (Ando et al., 2012; Audet et al., 2009; Fagereng & Sibson, 2010; Kaproth & Marone, 2013; Kodaira et al., 2004; Lavier et al., 2013; Liu & Rice, 2007; Segall et al., 2010; Shibazaki & Iio, 2003). Thus, the relationship between SSEs and seismicity at the Hikurangi margin is an active topic of investigation. Several studies show a strong linkage between microseismicity rates and shallow SSE occurrence at Hikurangi (Bartlow et al., 2014; Delahaye et al., 2009; Wallace et al., 2017; Wallace, Beavan, et al., 2012), and others have shown evidence for tremor concurrent with SSEs at north Hikurangi (Kim et al., 2011; Todd et al., 2018; Todd & Schwartz, 2016). The ability to locate offshore earthquakes, important for better understanding Hikurangi subduction zone processes, has been hampered by the lack of offshore seismic stations.

In this paper, we present an earthquake catalog for the Raukumara Peninsula region of the Hikurangi Margin, New Zealand, developed using the data from the May 2014 to June 2015 HOBITSS experiment (Wallace et al., 2016) in conjunction with land seismometers of the New Zealand National Seismograph Network maintained by GeoNet (www.geonet.org.nz). We investigated the hypocentral distribution of earthquakes on the plate boundary interface and within the subducting plate, taking advantage of a deployment that allows us to better pinpoint where the offshore seismicity is located and then explored the spatial and temporal variations of seismicity before, during and after the large SSE of September–October 2014.

2. Data and Methods

2.1. Data

The HOBITSS experiment consisted of 15 ocean bottom seismometers and 24 seafloor pressure gauges deployed in a dense array (6- to 22-km spacing) offshore Gisborne and Mahia Peninsula, New Zealand, from May 2014 to June 2015 (Figure 2). Most of the instruments were located on the offshore outer forearc (overriding plate), with a few instruments seaward of the trench on the incoming Pacific Plate (Figure 2). The network included ocean bottom seismometers (OBS) and APGs provided by United States and Japanese institutions and was augmented with the permanent land seismometers operated by GeoNet (Table S1; Petersen et al., 2011). OBS instruments included 10 broadband seismometers from Lamont Doherty Earth Observatory (LDEO-NY, USA) with a sampling rate of 100 samples per second (sps) and five short period seismometers from Earthquake Research Institute (Japan) with a sampling rate of 200 sps (see Table S1). Most of the LDEO OBS instruments also had an APG and a hydrophone channel. Sample seismograms are shown in Figure 3. The LDEO APGs and instruments with a hydrophone channel could be used for picking *P* waves of some of the local earthquakes with higher magnitude or hypocenters in close proximity to the APGs. Further information on the performance and characteristics of the instruments can be found in the supporting information.

2.2. Data Processing and Initial Locations

We compiled the land and ocean seismic waveform data in the Antelope relational database (Boulder Real Time Technologies, Inc.—www.brtt.com) for the initial analysis. First, phase arrivals were detected and preliminary locations were established for the period between 17 May 2014 and 21 June 2015. We used a short-term average/long-term average amplitude ratio (STA/LTA) algorithm on bandpass filtered (3–50 Hz) continuous vertical component data to detect preliminary *P* wave arrivals. Window lengths of 1 s for the STA and 5 s for the LTA window were used, and a STA/LTA ratio of at least 3.5 was required to declare a detection. We then performed a grid search over possible hypocenter locations to associate the individual detections with a potential event, requiring an association of a minimum of four detections (stations) to declare an event. The detection and subsequent event association processes yielded 7,000 potential seismic events. Each potential event was manually inspected, *P* and *S* wave arrival times were picked manually (only *P* phases when using a pressure channel or instrument), and uncertainties were assigned. Bad associations were also removed (root-mean-square (RMS) residual higher than 1.0 or clear phase arrivals at fewer than four stations). Earthquake locations were determined using GENLOC (Pavlis et al., 2004) with the iasp91 velocity model (Kennett & Engdahl, 1991) used for initial solutions. Preliminary locations outside the study area (green box in Figure 1) were ignored. The preliminary location process resulted in hypocenters for 2,619 earthquakes. Figure 3 shows an example of the *P* and *S* arrivals picked in the different instruments in this experiment, for a M_L 2.93 earthquake.

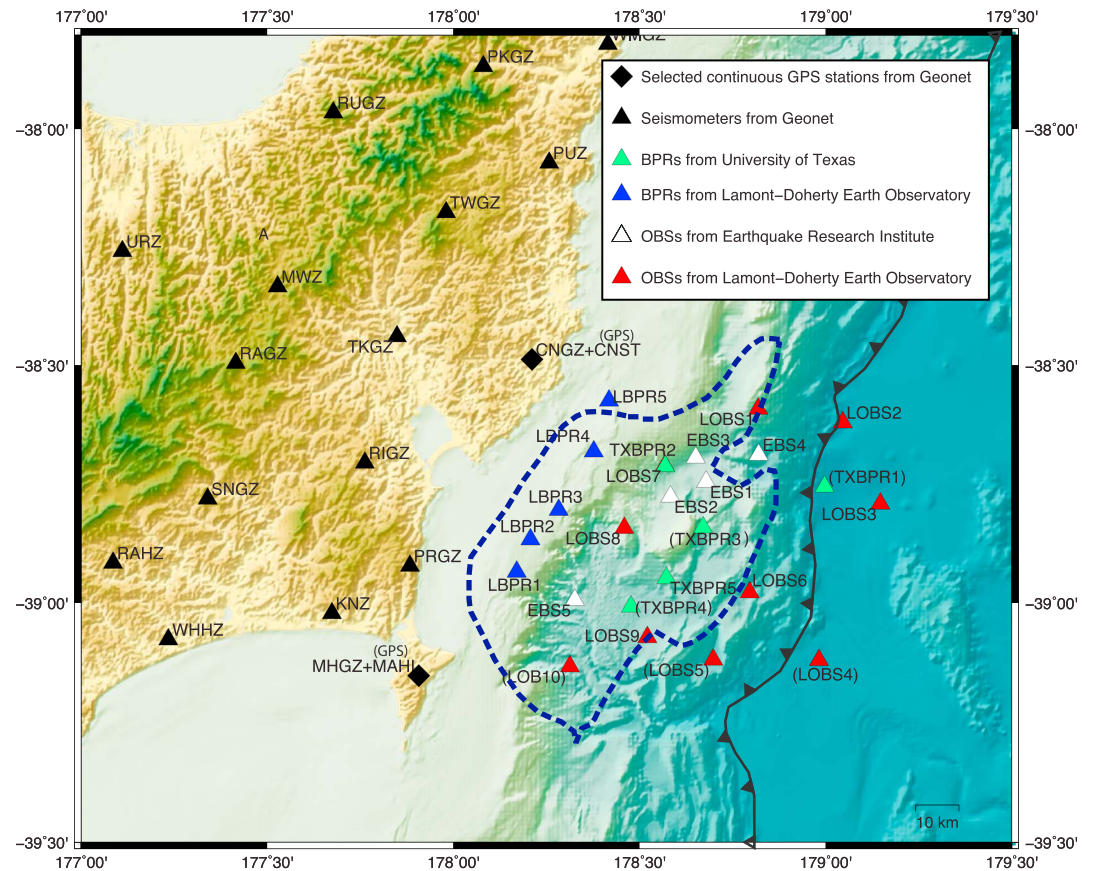


Figure 2. HOBITS and GeoNet stations used in this study. Stations in parenthesis indicate where no useful data were recovered. Grey dashed line A-A' to indicate cross section in Figures 8 and 10. Dark blue dashed line indicates the main area of the 2014 SSE (50-mm slip contour). Instrument performance details are given in the supporting information. Gray line with triangles indicates location and direction of the Hikurangi trench and subduction. OBS = ocean bottom seismometers.

Local magnitudes (M_L) for the 2,619 preliminary earthquakes were determined with Antelope's `dbvproc` tool. This program performs a local magnitude calculation by converting the raw data to a Wood-Anderson seismograph response, measuring event amplitude, and applying an attenuation-distance correction. We compute the largest amplitude of the S phase arrival on the horizontal components in a time window of 30 s, scale the magnitude based on hypocentral distance following an attenuation model for New Zealand (Ristau et al., 2016) in which the amplitude of the trace A_o (in millimeters) at each station (with no station correction) can be calculated as

$$\log A_o(R) = 0.29 - (1.27 \times 10^{-3})R - 1.49 \log(R)$$

(Ristau et al., 2016) where R is the hypocentral distance in kilometers. Local magnitude M_L is computed at each station that recorded a given event and the final magnitude is the average of these values. On average our local magnitude calculations are 0.32 units smaller than the equivalent GeoNet local magnitudes (Figure S2). GeoNet local magnitudes have been observed to be biased upward with respect to M_W by 0.34 units (Oth & Kaiser, 2014; Ristau, 2013), which is consistent with our observations.

The largest magnitude event (M_L 4.73) in our catalog occurred on 19 December 2014 and was also the largest event reported by GeoNet (M_L 4.97) during the same time period within the area of the HOBITS array. This event occurred at the beginning of a second large SSE (spanning from late December 2014 to early January 2015) located just to the south of the HOBITS array. Using the interactive GISMO MATLAB toolbox (Thompson & Reyes, 2017), we estimated a minimum magnitude of completeness (M_C) of our catalog of

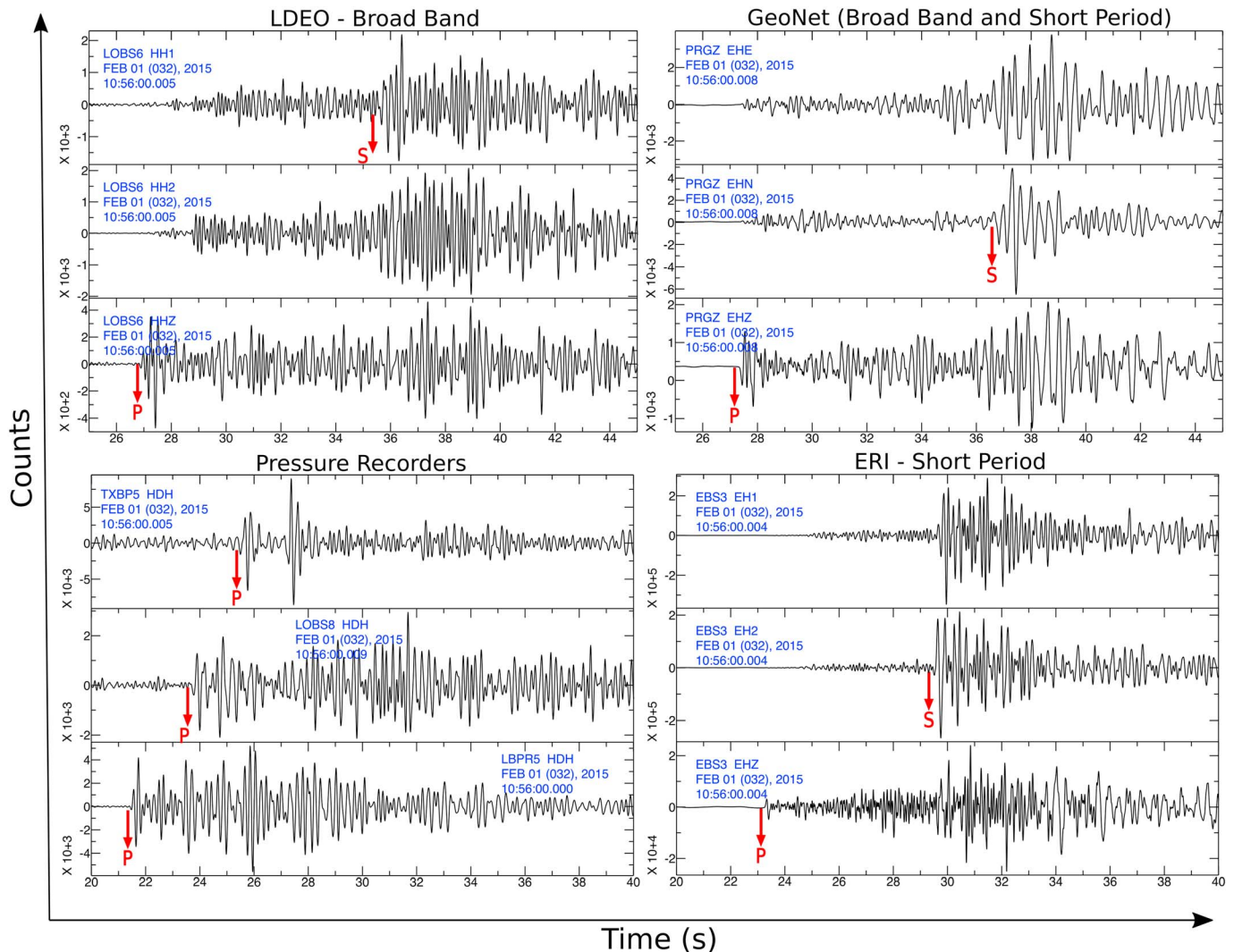


Figure 3. Example seismogram for an event recorded during HOBITSS deployment registered in short period and broadband seismometers as well as on APGs. Seismogram for 1 February 2015 earthquake, M_L 2.93. LDEO = Lamont Doherty Earth Observatory, ERI = Earthquake Research Institute.

M_L 1.5, following the method of the point of maximum curvature of the frequency-magnitude distribution for the estimated local magnitudes (Wiemer & Wyss, 2000; Figure 4). The slope of the linear Gutenberg-Richter relation yields a b -value of 0.80 ± 0.02 from the slope of the cumulative curve in Figure 4. The global average b -value is closer to 1.0 (Stein & Wysession, 2003), though lower b -values in subduction zone regions are not uncommon (Ghosh et al., 2008). Low b -values have been interpreted to indicate areas of high differential stress, such as at a plate interface that is highly coupled (locked; Ghosh et al., 2008; Öncel et al., 1996). Although the maximum curvature method has been found to underestimate the M_C (Woessner & Wiemer, 2005), which might affect the b -value estimation, we use M_C as a reference point to compare with the GeoNet catalog and to extract the most reliable part of the set of earthquakes and analyze their spatial and temporal distributions.

2.3. 1-D Velocity Model Determination

The tectonic complexity and lateral heterogeneity of the study area leads to marked differences in seismic velocity structure, so we determined separate 1-D velocity models for the onshore and offshore areas. Full 3-D seismic velocity inversion will be the subject of a future study. Our division between onshore and offshore regions resulted in 1,330 events onshore with 9,732 P arrivals and 9,265 S arrivals and 1,318 events offshore with 8,200 P arrivals and 8,003 S arrivals. We constructed Wadati diagrams for onshore stations with

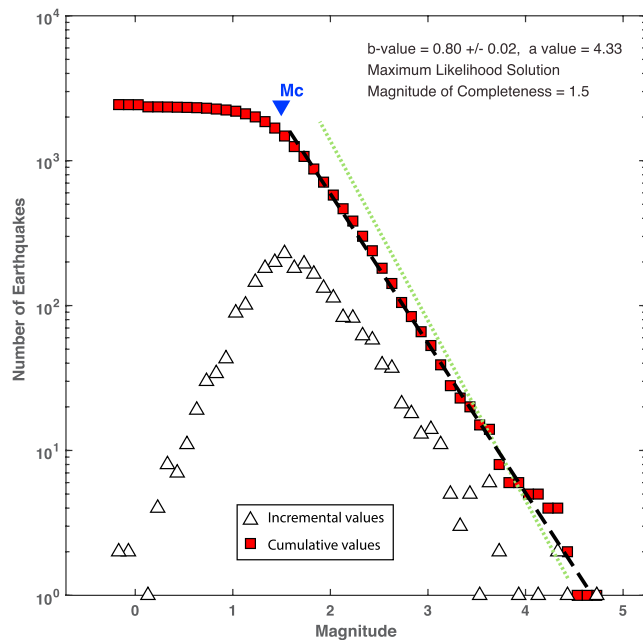


Figure 4. Frequency-magnitude plot for all earthquakes detected in the HOBITSS array for the entire area of study. Solid red squares mark the cumulative Gutenberg-Richter curve for number of earthquakes with greater magnitude M_L . Open black triangles mark the curve for incremental values in 0.1 $\text{Log}(M_L)$ magnitude unit bins. Inverted triangle labeled M_c denotes the point of maximum curvature. Black dashed line shows the resulting b value of 0.8 and the green dotted line a b value of 1.0 for reference.

onshore seismic events and offshore stations with offshore earthquakes and found V_p/V_s ratios of 1.75 for the NZ1D onshore and 1.76 for NZ1D offshore (Figure 5). For comparison, V_p/V_s ratios from the 3-D study by Eberhart-Phillips and Bannister (2015) ranged from 1.75 to 1.80 in this area. We next built 1-D velocity models for onshore and offshore settings (here NZ1D onshore and NZ1D offshore, respectively) using the Velest program (Kissling et al., 1994) and utilizing the V_p/V_s values from our Wadati diagrams as an a priori constraint for the resulting velocity model. The Velest program simultaneously inverts for the minimum 1-D velocity model, station correction, and hypocenter location (Kissling et al., 1994).

Velest requires a starting model that we set up for each region (onshore and offshore). We set these initial velocity models by combining available information from active and passive seismic experiments (Bassett et al., 2010, 2014; Reyners et al., 2006; Scherwath et al., 2010), and local and regional seismic tomography images (Eberhart-Phillips et al., 2010; Haijima, 2015; Stern et al., 2010). Our initial velocity models follow those of Bassett et al. (2010; offshore) and Stern et al. (2010; onshore) for the crust and subducting slab velocities (Table S2). The starting models we used were simple and represented the most important lithologic features: sediment layer, upper and lower crust, and subduction slab crust and mantle. Since Velest can only process a maximum of 658 earthquakes in the simultaneous mode, we decided to use the 500 largest events from each of the onshore and offshore preliminary earthquake locations (magnitudes between 1.7 and 4.7), which provide arrivals with good quality signals. We did not allow the Velest solution to contain low velocity layers as they have a strong effect on the raypaths and can introduce instabilities in the inversion process. We reached the minimum 1-D velocity model by trial and error of slight variations of faster/slower velocities and applica-

tion of different damping coefficients for the whole model and for specific layers. Our criteria to choose our final velocity model was based on the minimum average residual and minimal RMS misfit distribution of the 500 events used for each region. We set the base of our model to 150-km depth and below this depth we used the iasp91 model (Kennett & Engdahl, 1991). Figure 6 and Table S2 show the starting velocity models,

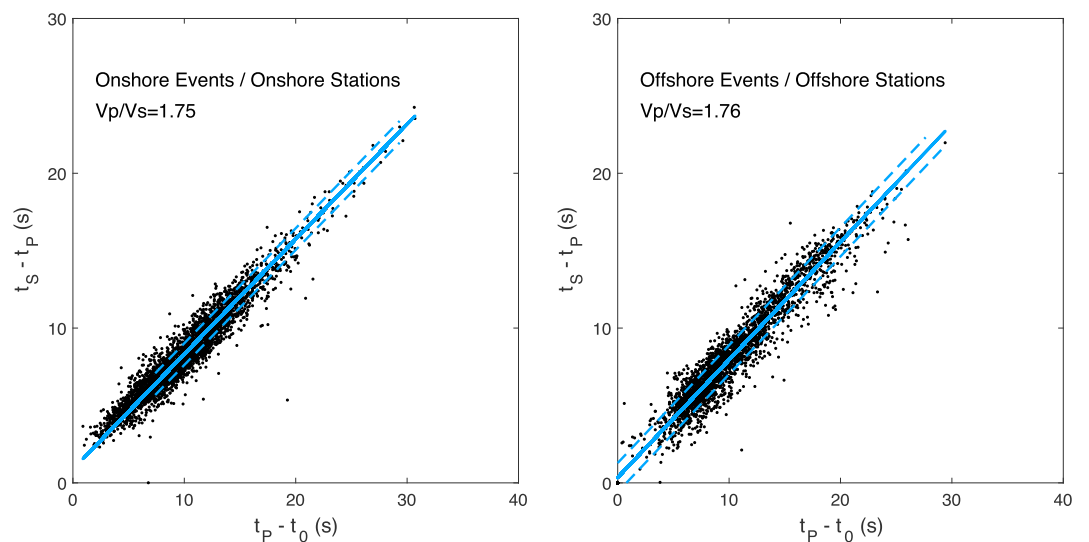


Figure 5. Wadati diagrams for the catalog for onshore and offshore events, separated by onshore and offshore stations. Solid blue line is the linear regression of event-station points with a slope of $(V_p/V_s - 1)$. Dashed blue lines correspond to the 95% confidence bounds.

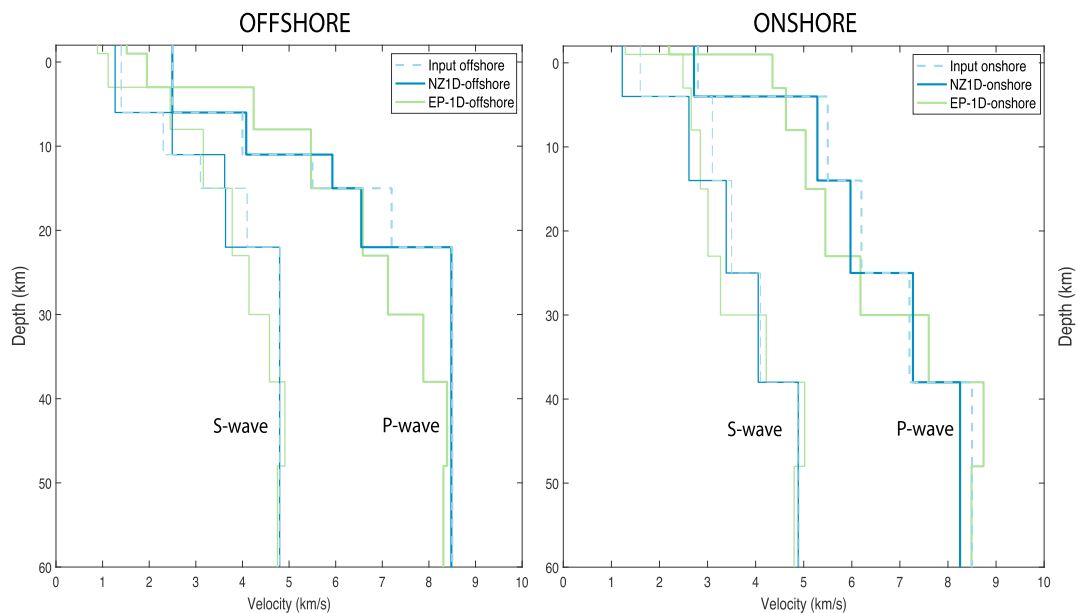


Figure 6. One-dimensional velocity models from inversion of HOBITSS and GeoNet data. Starting (input) models are described in text. EP-1D is a 1D version centered in each area of the 3-D velocity model of (Eberhart-Phillips et al., 2010).

the final minimum 1-D velocity model after Velest, and a 1-D version of each region of the 3-D velocity model of Eberhart-Phillips et al. (2010); here named EP-1D-onshore and EP-1D-offshore for comparison with our results. We observed that for the model NZ1D offshore, above 23-km depth (where the offshore Moho is located) the velocities of both starting and final models are slower than EP-1D-offshore, with differences up to 1.5 km/s. The shallowest and deepest final velocity layers do not change much with respect to the starting model. The layers that correspond to the upper crust, lower crust, and subducting slab differ from the starting model with slightly slower, slower and faster velocities, respectively. The slower velocities of NZ1D-offshore compared to EP-1D-offshore are expected to yield shallower hypocenter solutions than those published by GeoNet using the Eberhart-Phillips et al. (2010) model, particularly for events shallower than 20-km depth. On the other hand, NZ1D-onshore presents in general slightly faster velocities than EP-1D-onshore except for the shallowest layer (Figure 6). Our offshore results are broadly consistent with new results from an offshore active source experiment in this region (Bassett et al., 2018).

2.4. Event Relocation

We used the hypocenter location algorithm Bayesloc (Myers et al., 2007, 2009) along with our locally determined velocity models from Velest to improve upon our initial hypocenters. Bayesloc uses a Bayesian hierarchical statistical method to solve for multiple event hypocenter locations. It calculates a joint probability distribution on the arrival data completed via the Markov Chain Monte Carlo sampling method (Myers et al., 2007). This tool has the advantage of quantifying uncertainties, allowing us to evaluate the confidence for each location. We relocated 2,619 events using the NZ1D-onshore and NZ1D-offshore velocity models using the arrival table in Bayesloc. The 277 events were manually removed due to a very anomalous depth with large residuals, and 29 outlier events were automatically removed during inversion due to mispicks and/or travel time solutions that are outside the acceptance values for the multi-event location mode in Bayesloc (Myers et al., 2007, 2009). Our relocation resulted in 2,313 retained events, with 535 of the events within the HOBITSS deployment area (2014 SSE main area).

Histograms of standard deviations for hypocenter determination differentiated by offshore, onshore, and whole catalog distributions are shown in Figure S3. Deviations for epicentral solutions (latitude and longitude) present most of the deviation around 2 km with a slightly larger uncertainty for epicenters located offshore. Depth deviations present more differences between offshore events and the rest of the catalog. Results also show a peak of depth deviation around 3 km for both catalogs but with a much wider uncertainty for

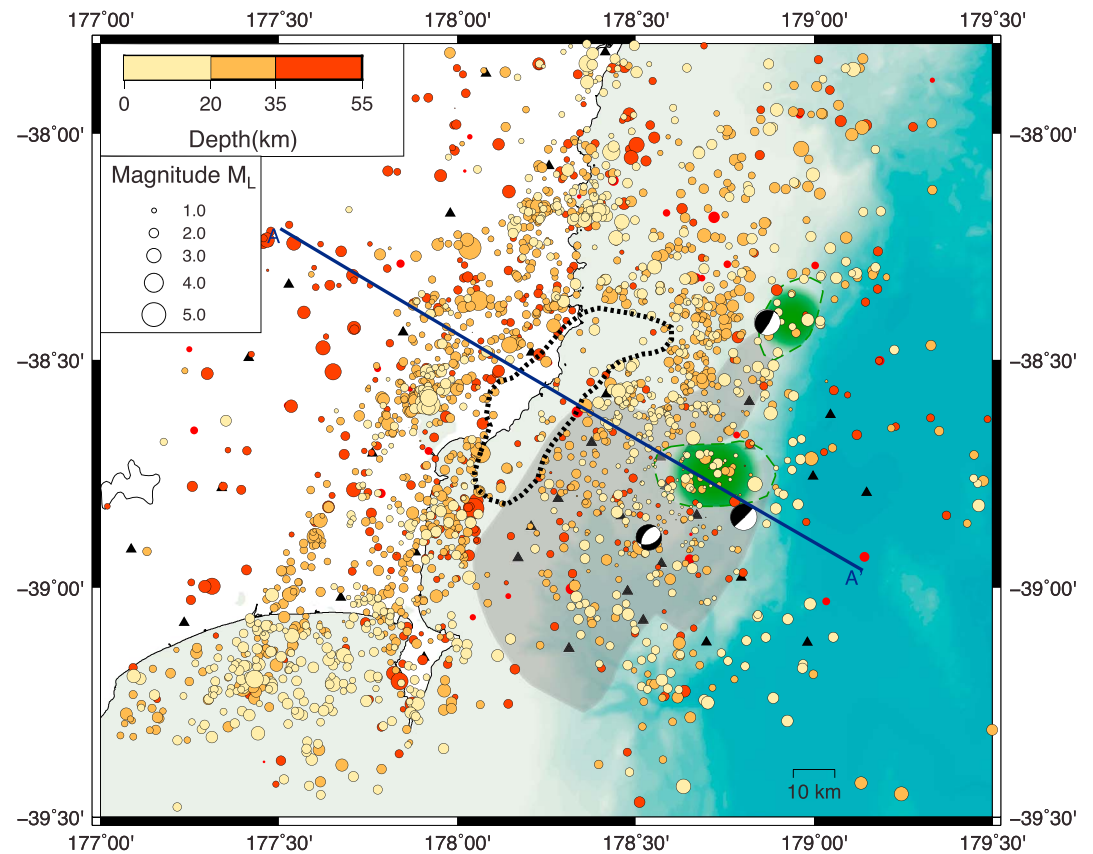


Figure 7. Hypocenters determined using Bayesloc with NZ1D onshore and NZ1D offshore velocity models. Event symbol is scaled by local magnitude size and colored by depth. Gray shaded area encloses the September–October slow slip area. Focal mechanisms show two M_w 7.0 1947 earthquakes and the M_w 6.7 December 2007 earthquake. Black triangles are HOBITSS and GeoNet stations. Shaded green areas surrounded by dashed lines are locations of detected seamounts. Black dotted line encloses the area of seismicity gap.

hypocenters offshore that reach maximum deviations around 15 km. Besides the advantage of using OBSs offshore, true depth solutions of small earthquakes are still a challenge that depends on velocity model, seismometer array distribution and the inevitable observational uncertainties.

3. Results

An obvious advantage of our OBS deployment is enhanced event detection and location capabilities in the offshore region and improved azimuthal coverage for coastal events. Using the 35,209 manual *P* and *S* phase picks (17,939 and 17,270, respectively), we found almost twice as many earthquakes detected in this study area (2,313 events) compared to the same period of time (May 2014 to June 2015) as reported by GeoNet (1,325 events). Considering just the events located offshore in the area of the HOBITSS deployment (see inset map in Figure 9), we found in this experiment that the number of events reported by GeoNet (373 events) is less than half the number of offshore events found in this study (950 events). A comparison of the magnitudes of completeness for both data sets shows that our catalog confidently detects events above M_L 1.5, while GeoNet's magnitude of completeness varies from 1.8 for onshore events to 2.2 in the offshore portion of the catalog (Table S3). This enhanced catalog aids in our understanding of seismicity in this important area of shallow slow slip (an area that also poses a large earthquake and tsunami hazard), due to a greater azimuthal coverage and the location of seismometers offshore overlying much of the slow slip area (Figure 2).

Our results (Figure 7) indicate that seismicity in the 1-year interval is concentrated in two NE-SW trending bands (parallel to slab strike), one offshore beneath the outer forearc wedge, one onshore beneath the

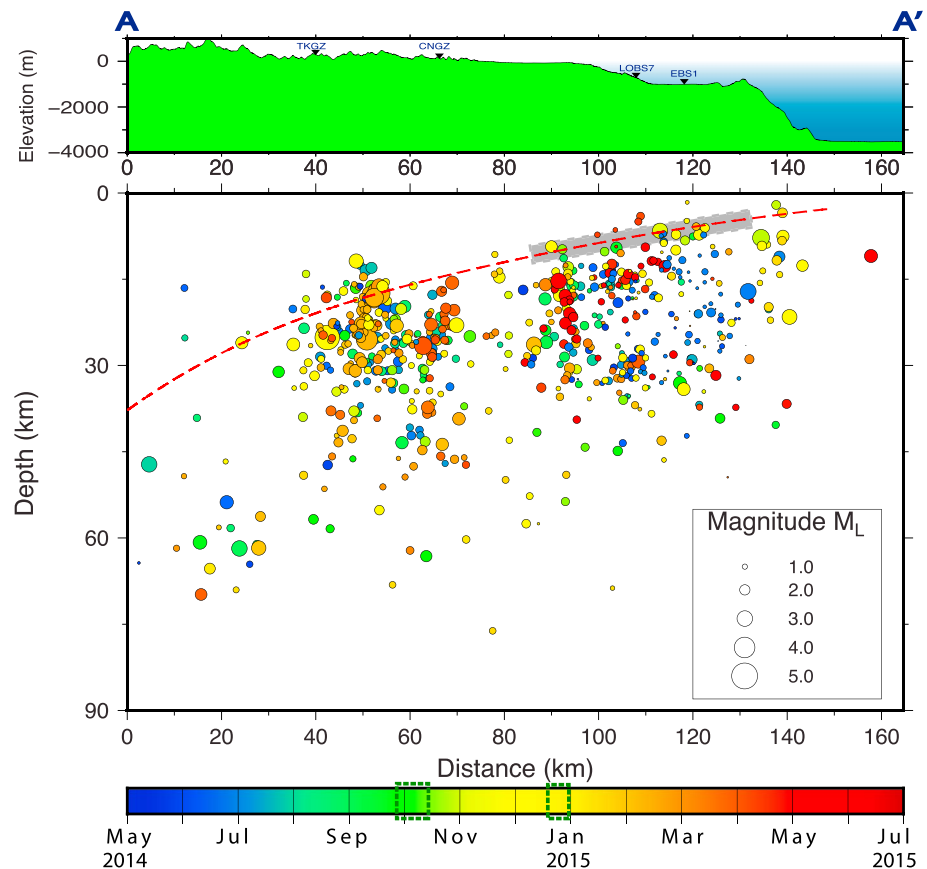


Figure 8. Cross section across the Hikurangi margin for hypocenters located in a 20-km width range on each side of vertical plane defined by A–A' in Figure 7. Earthquakes are color coded by date of occurrence. Green dashed rectangles in the time scale bar shows the September–October and the December SSEs. Red dotted line is the subduction zone plate interface from Williams et al. (2013). Gray box over the plate interface shows the location of the September–October 2014 SSE.

eastern Raukumara Peninsula, and with a clear gap in microseismicity between the two bands beneath the inner forearc wedge that extends throughout the subducting slab. The 20-km-wide seismicity gap is at the downdip edge of the offshore seismicity beneath the outer forearc. A similar gap is also observed from events in the GeoNet catalog (Figure S1). Offshore, earthquakes are mainly concentrated in the 15- to 25-km depth range, near and below the subduction zone interface proposed by Williams et al. (2013) as well as within the subducting Pacific plate with depth increasing to the west. Onshore, the earthquakes trend NE–SW at depths from 25 to 40 km, with several concentrated earthquake clusters, and sparser seismicity from 40- to 80-km depth. There is no clear trend in the magnitude distribution nor in the broader temporal distribution of the earthquakes (Figures 7 and 8).

4. Discussion

This study produces a yearlong catalog of microseismicity for the northern Hikurangi margin, including seismicity before, during, and after the October 2014 SSE offshore Gisborne, New Zealand. Our catalog also encompasses the time of a second large SSE offshore Mahia Peninsula (in the southern portion of our network) from approximately 18 December 2014 to 1 January 2015. A comparison of our hypocenters to those of GeoNet reveal small differences for onshore events (typically <5 km) and significant differences for offshore events (differences up to 30 km; Figures 9 and S4), which is not surprising given the improved offshore array coverage provided by the HOBITSS network as well as differences in velocity models. In the area centered on our offshore array of stations, HOBITSS hypocenters tend to relocate to the NW and shallower than GeoNet solutions for the same earthquakes (Figures 9 and S4). This shallower trend can be partially

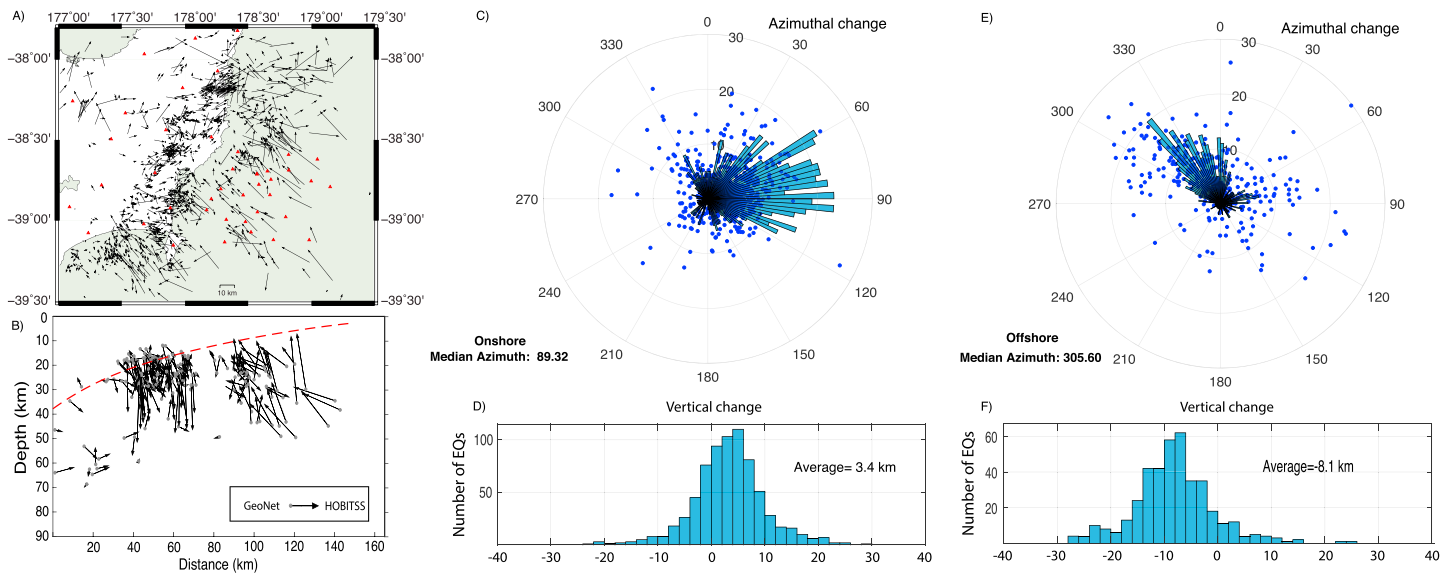


Figure 9. Changes in earthquake location from Geonet to our relocation solution, for events both in GeoNet catalog and our catalog. Red triangles indicate stations. A) map view, B) cross section. In both cases arrows point from GeoNet location to HOBITSS location. C) and E) polar plot histograms of azimuthal frequency of change in bins of 3°. Blue dots are single earthquake horizontal distance change (radial axis) and azimuthal change (angular axis). D) and F) are histograms for vertical shift in hypocenter location (negative represents shallower shift while positive represents deeper shift). HOBITSS = Hikurangi Ocean Bottom Investigation of Tremor and Slow Slip.

explained by the lower velocities in the upper crust in our models (Figure 6) relative to the velocity model used by GeoNet (Eberhart-Phillips et al., 2010), as well as the broader spatial distribution of our seismometers including their close proximity to offshore events. The offshore earthquakes are outside of the GeoNet network, and there is a well-known tradeoff between depth and origin time, explaining some of the large differences between our hypocenters compared to GeoNet. Our hypocenters indicate that many of the earthquakes are closer to the subduction interface (Williams et al., 2013) than the ones reported by GeoNet for this part of the Hikurangi margin. This comparison is intended to illustrate systematic location biases and aid in interpretation of offshore earthquake hypocenters that are determined using only onshore stations. Thus, this offset analysis (Figures 9 and S4) may be used as an aid in interpreting the GeoNet catalog for years when an offshore network was not available.

Contrasting physical properties of the sediments and bathymetric features on the incoming plate likely play a role in influencing the distribution of seismicity, tremor, and SSEs observed in the Hikurangi subduction zone. The subducting Hikurangi Plateau has rough bathymetry with seamounts exposed in the seafloor east of the trench (Figure 2) and subducted seamounts that are imaged in seismic reflection profiles and magnetic anomalies (Barker et al., 2018; Bell et al., 2010). The sediments overlying the Plateau comprise a 1- to 2-km-thick sequence of turbidites and pelagic sediments, as well as likely Cretaceous age volcanoclastics and sediments at the base of the sedimentary sequence (Davy et al., 2008). Down-dip of the subducting seamounts, high-amplitude reflectivity zones have been interpreted as tectonically eroded and underthrust fluid-rich sediments, up to a few kilometer thick (Bell et al., 2010). Subducted sediments can contribute to reductions in effective stresses (increasing high pore fluid pressure), which may also play a role in stimulating SSEs (Barker et al., 2018; Bell et al., 2010).

This microseismicity catalog can additionally reveal heterogeneities in the subducting plate, consistent with previous observations and directly relevant to seismicity patterns. The regions down-dip of the seamounts have been found to have high electrical conductivities (Heise et al., 2017; though they note low resolution in the offshore region), high V_p/V_s ratios (Eberhart-Phillips & Bannister, 2015), and low ratios of shear and compressional seismic wave attenuation ($Q_s/Q_p < 1$; Eberhart-Phillips et al., 2017). These areas have been interpreted as regions of high fluid pressure at the plate interface, facilitating aseismic creep and SSEs (Eberhart-Phillips et al., 2017; Eberhart-Phillips & Bannister, 2015; Heise et al., 2017; Figure 10). Focal mechanisms in the HOBITSS area show both normal and strike-slip mechanisms (Chon et al., 2016;

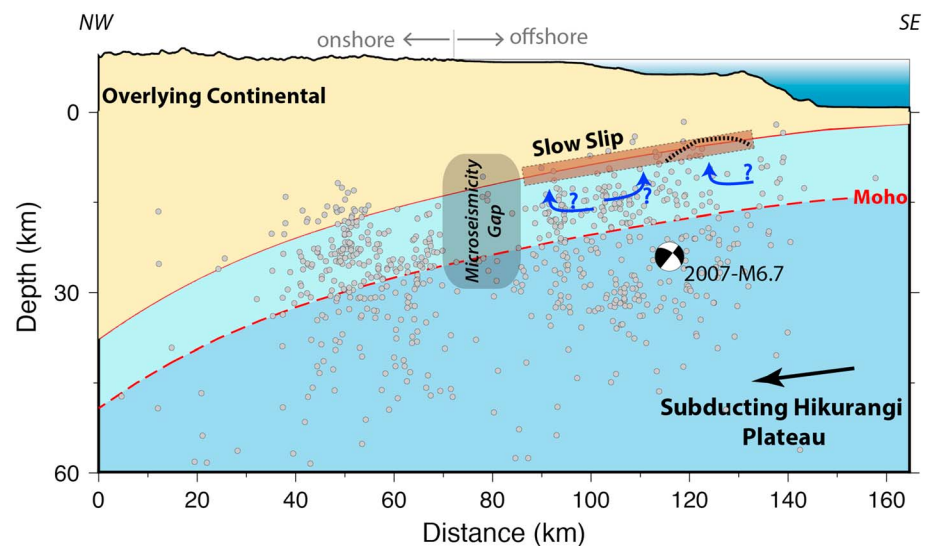


Figure 10. Schematic cross section with hypocenter location of the downdip and updip intraplate seismicity (grey dots), the main slow slip area (>50 mm), the seismic gap, the estimated oceanic Moho from Davy et al. (2008) and Hoernle et al. (2010), and the location of a seamount (black dotted line) from Bell et al. (2010). Blue arrows paths represent upward migration of fluids. Focal mechanism is the 2007 M_W 6.7 earthquake event.

Warren-Smith, Fry, Chon, et al., 2018; Figure S1). Previous focal mechanism studies in the area have interpreted the normal faulting events as evidence of bending stresses imposed by the flexure of the lithosphere (Bannister et al., 1989; Webb & Anderson, 1998). Focal mechanisms in the study area from different sources can be found in Figure S1 (Doser & Webb, 2003; Dziewonski et al., 1981; Ekström et al., 2012; François-Holden et al., 2008; and GeoNet moment tensors). The abundant offshore intraslab seismicity in the Hikurangi subducting crust may indicate an extensional section of the subducting slab fractured by the bending stresses related to the downgoing plate, which could enable upward migration of fluids to sustain elevated pore fluid pressure and potentially promote SSE occurrence as suggested by Eberhart-Phillips and Bannister (2015). In the onshore region, the seismicity is located in the lower continental crust, the plate interface, and the upper subducting slab (Figure 8). Beneath the onshore region, electrically resistive patches have been interpreted as an interface shear zone with reduced fluid or sediment content which can increase frictional coupling for this section of the interface (Heise et al., 2017). V_p/V_s and Q_s/Q_p ratios show intermediate values in the region of onshore intraplate seismicity between 15- and 40-km depth (Eberhart-Phillips et al., 2017; Eberhart-Phillips & Bannister, 2015). The heterogeneity in geophysical observables suggests that the Hikurangi subduction, at least for this portion of the margin, is a collection of coupled, creeping, and slow slip patches that play an important role in defining the distribution of seismicity, tremor, and SSEs.

Our earthquake locations confirm the presence of an offshore microseismicity gap, located northeast of Gisborne in 2014–2015 (Figures 7 and 8), also observed in the 2007–2016 GeoNet catalog (Figure S1). The region we refer to as a microseismicity gap is a region with low microseismicity surrounded by a region of high microseismic activity not unlike what has been referred to as a “Mogi doughnut” in the past (Kanamori, 1981; Mogi, 1968; Shearer & Lin, 2009). This 20-km-wide gap is at the down-dip edge of the 2014 SSE, and this region also coincides with areas with low Q_p/Q_s and intermediate V_p/V_s (Eberhart-Phillips et al., 2017). Some hypotheses detailed below can be proposed to explain the presence of this plate-wide intraslab seismicity gap: (1) Interseismic locking of the interface and intraplate faults could result in a temporary gap in microseismicity. Interplate coupling areas (or sections of interface showing high slip deficit and elastic strain accumulation) coincide with the location of the microseismicity gap (Dimitrova et al., 2016; Wallace et al., 2009). This coupling might be locally enhanced by a fluid- and sediment-starved interface area that creates higher frictional conditions. (2) Another possibility is that the seismicity gap is a consequence of spatially heterogeneous fluid transfer or changing permeability between the slab and the upper plate (Ingebritsen, 2013; Kano et al., 2018; Kato et al., 2004). These hypotheses are not mutually



Figure 11. (bottom) Histogram (blue bars) of number of earthquakes per day with magnitudes greater than M_L 1.5 within the blue polygon in upper left corner inset map and monthly accumulation of earthquakes (black line). (top) GPS time series of east displacement for CNST and MAHI stations. The green shaded areas highlight the onsets of the 2014 September–October and December SSEs. Inset map in the upper left corner shows the seismicity, the main 2014 event slow slip area in green and the blue polygon encloses the offshore seismicity analyzed in this figure.

exclusive and the pattern of seismicity observed in this margin may derive from a combination of the two mechanisms. We favor the plate coupling hypothesis as the dominant mechanism, as this observation offers the simplest explanation for the local lack of microseismic events. Locked plates would prevent any displacement in internal fractures, faults, and/or in the slab interface. If this gap in microseismicity is related to plate coupling and stress accumulation (that may be influenced by the presence of seamounts), then this has major implications for earthquake potential at the northern Hikurangi margin (Bell et al., 2014; Wallace et al., 2009).

We further investigated temporal variations in the seismicity patterns, particularly events in the region of the main slow slip area of the 2014 SSE, that were larger than the magnitude of completeness ($M_L > 1.5$). Relative to the background seismicity, we observed a slight increase in local microearthquake seismicity lasting for an interval of 2 months (Figure 11). This slight increase is also visible when the up-dip, down-dip, and SSE area subdivisions of the subducting slabs were additionally analyzed in terms of the temporal distributions (Figure S5). The start of the increase in seismicity rate coincides with the September–October 2014 SSE and continues at a similar rate after the SSE, eventually decaying a few days after the December 2014 event. Todd et al. (2018) and Iwasaki et al. (2017) report abundant offshore tremor activity that also peaked after the 2014 SSE. Todd et al. (2018) manually scanned HOBITSS and GeoNet data and located all events within the network occurring in a 2 month period spanning the 2014 SSE (September and October 2014). Their catalog for this 2 month period reveals a similar increase in seismic activity toward the end of second SSE. Some previous SSEs (such as the 2004 and 2010 Gisborne SSEs) have produced a clearer increase in seismicity rate changes during north Hikurangi SSEs (Delahaye et al., 2009; Jacobs et al., 2016; Todd & Schwartz, 2016). Similar patterns of microearthquake seismicity relative to the 2014 SSE have been observed in southern Mexico, where an increase in rates of seismicity occurred during an SSE that preceded the 2012 M_w 7.4 Ometepec earthquake (Colella et al., 2017). La Plata Island (Ecuador) SSEs also have shallow SSEs (10- to 15-km depth), similar to north Hikurangi; a sharp increase in local seismicity has been observed during a 2010 SSE in the Central Ecuador Subduction zone (Vallée et al., 2013). However, other shallow slow slip examples in Costa Rica and Nankai, Japan, show different patterns of seismicity from the one described in this study. The Costa Rica SSEs are found to be well correlated in time with seismic tremor despite not being correlated in space, with no detectable increase in microearthquake seismicity (Outerbridge et al.,

2010). Also contrary to the 2014 SSE, the 2013 SSE in the Nankai region observed with ocean bottom network of pressure recorders, exhibited a synchronous decrease in seismicity rate suggesting a close relationship between seismicity and SSEs (Suzuki et al., 2016). The Hikurangi margin SSEs have shown overlapping increases of seismicity and tremor activity during SSEs. However, other SSE regions present different patterns, suggesting that relationships of seismicity with SSEs may vary with specific subduction zone conditions.

The major seismological features that we observe and interpret for this part of the Hikurangi margin are illustrated in Figure 10. The spatial coincidence of the subducted seamounts, intense fracturing from bending stresses generating earthquakes from normal faults (acting as fluid pathways), and underthrusting of a thick pile of fluid-rich sediments are proposed to increase pore fluid pressure and potentially promote the onset of SSEs. The microseismicity gap is located at the downdip edge of the September–October 2014 SSE, and we suggest that it is related to a locked patch of the interface as indicated by the plate coupling results from geodetic modeling (Wallace, Barnes, et al., 2012). We observe a subtle temporal variation in seismicity coinciding and extending a few weeks beyond the 2014 SSE. Other researchers are further examining the temporal aspects of seismicity with enhanced catalogs focused on the slow slip region (e.g., Shaddock & Schwartz, 2019; Warren-Smith, Fry, Chon, et al., 2018).

5. Conclusions

We created a catalog of 2,313 earthquakes on and offshore Gisborne, North Island, New Zealand using ocean bottom seismometers from the 2014–2015 HOBITSS experiment and onland seismometer stations from GeoNet. The majority of earthquake hypocenters are located in the subducting Pacific plate and on the interface where the offshore SSEs occur. A small increase in seismicity is observed during the onset of the September–October 2014 SSE and continues to increase following the event for a few months, and tails off a month or two after a second SSE in the region in December 2014. Our seismicity locations also reveals a ~20-km-wide seismicity gap trending NE located just down-dip of the north Hikurangi slow slip area that exhibited aseismic creep in the September–October 2014 event. This gap in seismicity is persistent throughout the slab. The region of low microseismicity also coincides with a region of elevated and moderate interseismic coupling as determined from GPS (Wallace, Barnes, et al., 2012; Figure S6), suggesting the possibility that the gap in seismicity is a consequence of interseismic coupling on the plate boundary. Our interpretation also proposes that bending stress-generated faults hosting abundant offshore seismicity within the subducting plate enable the upward migration of fluids, increasing the pore fluid pressure on the interface above and creating optimal conditions for occurrence of SSEs.

References

- Ando, R., Takeda, N., & Yamashita, T. (2012). Propagation dynamics of seismic and aseismic slip governed by fault heterogeneity and Newtonian rheology. *Journal of Geophysical Research*, 117, B11308. <https://doi.org/10.1029/2012JB009532>
- Audet, P., Bostock, M. G., Christensen, N. I., & Peacock, S. M. (2009). Seismic evidence for overpressured subducted oceanic crust and megathrust fault sealing. *Nature*, 457(7225), 76–78. <https://doi.org/10.1038/nature07650>
- Bannister, S. C., Perin, B. J., & Webb, T. H. (1989). Normal faulting through subducted oceanic crust: the 19 July 1985 earthquake of Hawke's Bay, New Zealand. *Tectonophysics*, 162(3–4), 303–313. [https://doi.org/10.1016/0040-1951\(89\)90251-5](https://doi.org/10.1016/0040-1951(89)90251-5)
- Barker, D. H. N., Henrys, S., Caratori Tontini, F., Barnes, P. M., Bassett, D., Todd, E., & Wallace, L. M. (2018). Geophysical constraints on the relationship between seamount subduction, slow slip and tremor at the north Hikurangi subduction zone, New Zealand. *Geophysical Research Letters*, 45, 12,804–12,813. <https://doi.org/10.1029/2018GL080259>
- Barker, D. H. N., Sutherland, R., Henrys, S., & Bannister, S. C. (2009). Geometry of the Hikurangi subduction thrust and upper plate, North Island, New Zealand. *Geochimistry, Geophysics, Geosystems*, 10, Q02007. <https://doi.org/10.1029/2008GC002153>
- Bartlow, N. M., Wallace, L. M., Beavan, J., Bannister, S. C., & Segall, P. (2014). Time-dependent modeling of slow slip events and associated seismicity and tremor at the Hikurangi subduction zone, New Zealand. *Journal of Geophysical Research: Solid Earth*, 119, 734–753. <https://doi.org/10.1002/2013JB010609>
- Bassett, D., Henrys, S. A., Barker, D. H. N., Arnulf, A. F., Arai, R., Kodaira, S., et al. (2018). The relationship between forearc structure and geodetic locking along the Hikurangi margin from SHIRE seismic data. In *American Geophysical Union, Fall Meeting 2018, abstract id. T53C-07*.
- Bassett, D., Sutherland, R., & Henrys, S. (2014). Slow wavespeeds and fluid overpressure in a region of shallow geodetic locking and slow slip, Hikurangi subduction margin, New Zealand. *Earth and Planetary Science Letters*, 389. <https://doi.org/10.1016/j.epsl.2013.12.021>
- Bassett, D., Sutherland, R., Henrys, S., Stern, T., Scherwath, M., Benson, A., et al. (2010). Three-dimensional velocity structure of the northern Hikurangi margin, Raukumara, New Zealand: Implications for the growth of continental crust by subduction erosion and tectonic underplating. *Geochimistry, Geophysics, Geosystems*, 11, Q10013. <https://doi.org/10.1029/2010GC003137>
- Bell, R., Holden, C., Power, W., Wang, X., & Downes, G. (2014). Hikurangi margin tsunami earthquake generated by slow seismic rupture over a subducted seamount. *Earth and Planetary Science Letters*, 397, 1–9. <https://doi.org/10.1016/J.EPSL.2014.04.005>

Acknowledgments

The ocean bottom seismic data used in this research were provided by instruments from the Ocean Bottom Seismograph Instrument Pool (www.obsip.org) funded by the National Science Foundation (NSF), the Earthquake Research Institute (University of Tokyo), New Zealand's GeoNet project and its sponsors EQC, GNS Science, and LINZ that provided the land data in this study. Support for ship time was provided by NSF, GNS Science, and Land Information New Zealand's Oceans 2020 program. Support for data collection was provided by NSF grants 1333311, 1333025, 1332875, and 1334654, while analysis was provided by NSF grants 1551758, 1551683, and 1551922 and MBIE grant GNS-MBIE00053. Raw data from the experiment is archived and available to download at the Incorporate Research Institutions for Seismology Data Management Center with experiment codes YH 2014–2015 (seismic data) and 8F 2014–2015 (bottom pressure record data). The seismic catalog is publicly available at <https://zenodo.org/record/2022405#>. XibszRNKgWo website. We value the vital contribution to this project from ocean bottom instrument engineering teams at LDEO, UTIG, University of Tokyo, and Tohoku University, as well as the captains and crew of the U.S. R/V Roger Revelle and New Zealand's R/V Tangaroa. J. Y. extends thanks to Justin Ball for discussion that improved the manuscript. We thank Samantha Privett and Lauren Eng for the assistance in manual picking of the automated detections. We thank the editor and two anonymous reviewers for their constructive comments.

- Bell, R., Sutherland, R., Barker, D. H. N., Henrys, S., Bannister, S. C., Wallace, L. M., & Beavan, J. (2010). Seismic reflection character of the Hikurangi subduction interface, New Zealand, in the region of repeated Gisborne slow slip events. *Geophysical Journal International*, 180(1), 34–48. <https://doi.org/10.1111/j.1365-246X.2009.04401.x>
- Chon, E., Sheehan, A. F., Yancey, J., Nakai, J. S., Schwartz, S. Y., & Mochizuki, K. (2016). Focal mechanism solutions from the HOBITSS Ocean Bottom Seismometer Experiment, Hikurangi Subduction Zone, New Zealand. *American Geophysical Union, Fall Meeting 2016, Abstract #T31D-2927*. Retrieved from <http://adsabs.harvard.edu/abs/2016AGUFM.T31D2927C>
- Colella, H. V., Sit, S. M., Brudzinski, M. R., Graham, S. E., Demets, C., Holtkamp, S. G., et al. (2017). Seismicity rate increases associated with slow slip episodes prior to the 2012 *M*_w 7.4 Ometepe earthquake. *Earth and Planetary Science Letters*, 464, 35–45. <https://doi.org/10.1016/j.epsl.2016.12.032>
- Davy, B., Hoernle, K., Werner, R., Hoernle, K., & Werner, R. (2008). Hikurangi Plateau: Crustal structure, rifted formation, and Gondwana subduction history. *Geochemistry, Geophysics, Geosystems*, 9, Q07004. <https://doi.org/10.1029/2007GC001855>
- Delahaye, E. J., Townend, J., Reyners, M., & Rogers, G. (2009). Microseismicity but no tremor accompanying slow slip in the Hikurangi subduction zone, New Zealand. *Earth and Planetary Science Letters*, 277(1–2), 21–28. <https://doi.org/10.1016/j.epsl.2008.09.038>
- Dimitrova, L., Wallace, L. M., Haines, A., & Williams, C. (2016). High-resolution view of active tectonic deformation along the Hikurangi subduction margin and the Taupo Volcanic Zone, New Zealand. *New Zealand Journal of Geology and Geophysics*, 59(1), 43–57. <https://doi.org/10.1080/00288306.2015.1127823>
- Doser, D. I., & Webb, T. H. (2003). Source parameters of large historical (1917–1961) earthquakes, North Island, New Zealand. *Geophysical Journal International*, 152, 795–832. <https://doi.org/10.1046/j.1365-246X.2003.01895.x>
- Douglas, A., Beavan, J., Wallace, L. M., & Townend, J. (2005). Slow slip on the northern Hikurangi subduction interface, New Zealand. *Geophysical Research Letters*, 32, L16305. <https://doi.org/10.1029/2005GL023607>
- Dziewonski, A. M., Chou, T. A., & Woodhouse, J. H. (1981). Determination of earthquake source parameters from waveform data for studies of global and regional seismicity. *Journal of Geophysical Research*, 86(B4), 2825–2852. <https://doi.org/10.1029/JB086iB04p02825>
- Eberhart-Phillips, D., & Bannister, S. C. (2015). 3-D imaging of the northern Hikurangi subduction zone, New Zealand: Variations in subducted sediment, slab fluids and slow slip. *Geophysical Journal International*, 201(2), 838–855. <https://doi.org/10.1093/gji/ggv057>
- Eberhart-Phillips, D., Bannister, S. C., & Reyners, M. (2017). Deciphering the 3-D distribution of fluid along the shallow Hikurangi subduction zone using *P*- and *S*-wave attenuation. *Geophysical Journal International*, 211(2), 1032–1045. <https://doi.org/10.1093/gji/ggx348>
- Eberhart-Phillips, D., Reyners, M., Bannister, S. C., Chadwick, M., & Ellis, S. (2010). Establishing a versatile 3-D seismic velocity model for New Zealand. *Seismological Research Letters*, 81(6), 992–1000. <https://doi.org/10.1785/gssrl.81.6.992>
- Ekström, G., Nettles, M., & Dziewoński, A. M. (2012). The global CMT project 2004–2010: Centroid-moment tensors for 13,017 earthquakes. *Physics of the Earth and Planetary Interiors*, 200–201, 1–9. <https://doi.org/10.1016/j.pepi.2012.04.002>
- Fagereng, A., & Sibson, R. H. (2010). Mélange rheology and seismic style. *Geology*, 38(8), 751–754. <https://doi.org/10.1130/G30868.1>
- François-Holden, C., Bannister, S. C., Beavan, J., Cousins, J., Field, B., McCaffrey, R., et al. (2008). The *M*_w 6.6 Gisborne earthquake of 2007: Preliminary records and general source characterization. *Bulletin of the New Zealand Society for Earthquake Engineering*, (4). Retrieved from http://www.rpi.edu/dept/irpri/IPRPIpublications/2008/mccaffrey_gizborne_2008.pdf
- Ghosh, A., Newman, A. V., Thomas, A. M., & Farmer, G. T. (2008). Interface locking along the subduction megathrust from *b*-value mapping near Nicoya Peninsula, Costa Rica. *Geophysical Research Letters*, 35, L01301. <https://doi.org/10.1029/2007GL031617>
- Hajijima, D. (2015). Seismic activity and velocity structure in the Northern Hikurangi subduction zone offshore the North Island of New Zealand. Earthquake Research Institute, Department of Earth and Planetary Science, University of Tokyo.
- Heise, W., Caldwell, T. G., Bannister, S., Bertrand, E. A., Ogawa, Y., Bennie, S. L., & Ichihara, H. (2017). Mapping subduction interface coupling using magnetotellurics: Hikurangi margin, New Zealand. *Geophysical Research Letters*, 44, 9261–9266. <https://doi.org/10.1002/2017GL074641>
- Hoernle, K., Hauff, F., van den Bogaard, P., Werner, R., Mortimer, N., Geldmacher, J., et al. (2010). Age and geochemistry of volcanic rocks from the Hikurangi and Manihiki oceanic plateaus. *Geochimica et Cosmochimica Acta*, 74(24), 7196–7219. <https://doi.org/10.1016/j.gca.2010.09.030>
- Ingebritsen, S. E. (2013). *Geology of the Earthquake Source - A Volume in Honor of Rick Sibson*. A. Fagereng, V. G. Toy, J. V. Rowland, eds., 2011 The Geological Society Publishing House, Geological Society Special Publication 359, Bath UK 318 pp. Geofluids, 13: 95–97. <https://doi.org/10.1111/gfl.12015>
- Iwasaki, Y., Mochizuki, K., Ishise, M., Todd, E. K., Schwartz, S. Y., Henrys, S. A., et al. (2017). Continuous shear wave signals from around a subducted seamount following 2014 *M*_w 6.8 slow-slip event in the Hikurangi subduction margin offshore New Zealand. *American Geophysical Union, Fall Meeting 2017, Abstract #S54C-03*. Retrieved from <http://adsabs.harvard.edu/abs/2017AGUFM.S54C.03I>
- Jacobs, K., Savage, M. K., & Smith, E. (2016). Quantifying seismicity associated with slow slip events in the Hikurangi margin, New Zealand. *New Zealand Journal of Geology and Geophysics*, 59(1), 58–69. <https://doi.org/10.1080/00288306.2015.1127827>
- Kanamori, H. (1972). Mechanism of tsunami earthquakes. *Physics of the Earth and Planetary Interiors*, 6(5), 346–359. [https://doi.org/10.1016/0031-9201\(72\)90058-1](https://doi.org/10.1016/0031-9201(72)90058-1)
- Kanamori, H. (1981). The Nature of seismicity patterns before large earthquakes. In D. W. Simpson & P. G. Richards (Eds.), *Earthquake Prediction: An International Review* (pp. 1–19). Washington, D. C.: American Geophysical Union. <https://doi.org/10.1029/ME004p0001>
- Kano, M., Kato, A., Ando, R., & Obara, K. (2018). Strength of tremor patches along deep transition zone of a megathrust. *Scientific Reports*, 8(1), 3655. <https://doi.org/10.1038/s41598-018-22048-8>
- Kapoth, B. M., & Marone, C. (2013). Slow earthquakes, preseismic velocity changes, and the origin of slow frictional stick-slip. *Science (New York, N.Y.)*, 341(6151), 1229–1232. <https://doi.org/10.1126/science.1239577>
- Kato, A., Sakaguchi, A., Yoshida, S., Yamaguchi, H., & Kaneda, Y. (2004). Permeability structure around an ancient exhumed subduction-zone fault. *Geophysical Research Letters*, 31, L06602. <https://doi.org/10.1029/2003GL019183>
- Kennett, B. L. N., & Engdahl, E. R. (1991). Traveltimes for global earthquake location and phase identification. *Geophysical Journal International*, 105(2), 429–465. <https://doi.org/10.1111/j.1365-246X.1991.tb06724.x>
- Kim, M. J., Schwartz, S. Y., & Bannister, S. C. (2011). Non-volcanic tremor associated with the March 2010 Gisborne slow slip event at the Hikurangi subduction margin, New Zealand. *Geophysical Research Letters*, 38, L14301. <https://doi.org/10.1029/2011GL048400>
- Kissling, E., Ellsworth, W. L., Eberhart-Phillips, D., & Kradolfer, U. (1994). Initial reference models in local earthquake tomography. *Journal of Geophysical Research*, 99(B10), 19,635–19,646. <https://doi.org/10.1029/93JB03138>
- Kodaira, S., Iidaka, T., Kato, A., Park, J.-O., Iwasaki, T., & Kaneda, Y. (2004). High pore fluid pressure may cause silent slip in the Nankai Trough. *Science (New York, N.Y.)*, 304(5675), 1295–1298. <https://doi.org/10.1126/science.1096535>
- Langridge, R., Ries, W., Litchfield, N., Villamor, P., Van Dissen, R., Barrell, D., et al. (2016). The New Zealand active faults database. *New Zealand Journal of Geology and Geophysics*, 59(1), 86–96. <https://doi.org/10.1080/00288306.2015.1112818>

- Lavier, L. L., Bennett, R. A., & Duddu, R. (2013). Creep events at the brittle ductile transition. *Geochemistry, Geophysics, Geosystems*, 14, 3334–3351. <https://doi.org/10.1002/ggge.20178>
- Liu, Y., & Rice, J. R. (2007). Spontaneous and triggered aseismic deformation transients in a subduction fault model. *Journal of Geophysical Research*, 112, B09404. <https://doi.org/10.1029/2007JB004930>
- McCaffrey, R. (2014). Interseismic locking on the Hikurangi subduction zone: Uncertainties from slow-slip events. *Journal of Geophysical Research: Solid Earth*, 119, 7874–7888. <https://doi.org/10.1002/2014JB010945>
- McCaffrey, R., Wallace, L. M., & Beavan, J. (2008). Slow slip and frictional transition at low temperature at the Hikurangi subduction zone. *Nature Geoscience*, 1(5), 316–320. <https://doi.org/10.1038/ngeo178>
- Mogi, K. (1968). Some features of recent seismic activity in and near Japan (1). *Bulletin of the Earthquake Research Institute*, 46(4), 1225–1236. Retrieved from. https://repository.dl.itc.u-tokyo.ac.jp/?action=pages_view_main&active_action=repository_view_main_item_detail&item_id=33369&item_no=1&page_id=28&block_id=31
- Myers, S. C., Johannesson, G., & Hanley, W. (2007). A Bayesian hierarchical method for multiple-event seismic location. *Geophysical Journal International*, 171(3), 1049–1063. <https://doi.org/10.1111/j.1365-246X.2007.03555.x>
- Myers, S. C., Johannesson, G., & Hanley, W. (2009). Incorporation of probabilistic seismic phase labels into a Bayesian multiple-event seismic locator. *Geophysical Journal International*, 177(1), 193–204. <https://doi.org/10.1111/j.1365-246X.2008.04070.x>
- Öncel, A. O., Main, I., Alptekin, Ö., & Cowie, P. (1996). Temporal variations in the fractal properties of seismicity in the North Anatolian Fault Zone between 31°E and 41°E. *Pure and Applied Geophysics PAGEOPH*, 147(1), 147–159. <https://doi.org/10.1007/BF00876441>
- Oth, A., & Kaiser, A. E. (2014). Stress release and source scaling of the 2010–2011 Canterbury, New Zealand earthquake sequence from spectral inversion of ground motion data. *Pure and Applied Geophysics*, 171(10), 2767–2782. <https://doi.org/10.1007/s00024-013-0751-1>
- Outerbridge, K. C., Dixon, T. H., Schwartz, S. Y., Walter, J. I., Protti, M., Gonzalez, V., et al. (2010). A tremor and slip event on the Cocos-Caribbean subduction zone as measured by a global positioning system (GPS) and seismic network on the Nicoya Peninsula, Costa Rica. *Journal of Geophysical Research*, 115, B10408. <https://doi.org/10.1029/2009JB006845>
- Pavlis, G. L., Vernon, F., Harvey, D., & Quinlan, D. (2004). The generalized earthquake-location (GENLOC) package: An earthquake-location library. *Computers & Geosciences*, 30(9), 1079–1091. <https://doi.org/10.1016/j.cageo.2004.06.010>
- Peng, Z., & Gomberg, J. (2010). An integrated perspective of the continuum between earthquakes and slow-slip phenomena. *Nature Geoscience*, 3(9), ngeo940. <https://doi.org/10.1038/ngeo940>
- Petersen, T., Gledhill, K., Chadwick, M., Gale, N. H., & Ristau, J. (2011). The New Zealand national seismograph network. *Seismological Research Letters*, 82(1), 9–20. <https://doi.org/10.1785/gssrl.82.1.9>
- Reyners, M., Eberhart-Phillips, D., Stuart, G., & Nishimura, Y. (2006). Imaging subduction from the trench to 300 km depth beneath the central North Island, New Zealand, with V_p and V_p/V_s . *Geophysical Journal International*, 165(2), 565–583. <https://doi.org/10.1111/j.1365-246X.2006.02897.x>
- Ristau, J. (2013). Update of regional moment tensor analysis for earthquakes in New Zealand and adjacent offshore regions. *Bulletin of the Seismological Society of America*, 103(4), 2520–2533. <https://doi.org/10.1785/0120120339>
- Ristau, J., Harte, D., & Salichon, J. (2016). A revised local magnitude (ML) scale for New Zealand earthquakes. *Bulletin of the Seismological Society of America*, 106(2), 398–407. <https://doi.org/10.1785/0120150293>
- Scherwath, M., Kopp, H., Flueh, E. R., Henrys, S. A., Sutherland, R., Stagpoole, V. M., et al. (2010). Fore-arc deformation and underplating at the northern Hikurangi margin, New Zealand. *Journal of Geophysical Research*, 115, B06408. <https://doi.org/10.1029/2009JB006645>
- Schwartz, S. Y., & Rokosky, J. M. (2007). Slow slip events and seismic tremor at circum-Pacific subduction zones. *Reviews of Geophysics*, 45, RG3004. <https://doi.org/10.1029/2006RG000208>
- Segall, P., Rubin, A. M., Bradley, A. M., & Rice, J. R. (2010). Dilatant strengthening as a mechanism for slow slip events. *Journal of Geophysical Research*, 115, B12305. <https://doi.org/10.1029/2010JB007449>
- Shaddox, H. R., & Schwartz, S. Y. (2019). Subducted seamount diverts shallow slow slip to the forearc of the northern Hikurangi subduction zone, New Zealand. *Geology*. <https://doi.org/10.1130/g45810.1>
- Shearer, P. M., & Lin, G. (2009). Evidence for Mogi doughnut behavior in seismicity preceding small earthquakes in southern California. *Journal of Geophysical Research*, 114, B01318. <https://doi.org/10.1029/2008JB005982>
- Shibazaki, B., & Iio, Y. (2003). On the physical mechanism of silent slip events along the deeper part of the seismogenic zone. *Geophysical Research Letters*, 30(9), 1489. <https://doi.org/10.1029/2003GL017047>
- Stein, S., & Wysession, M. (2003). *An introduction to seismology, earthquakes, and earth structure*. Malden, MA, USA: Blackwell Pub.
- Stern, T., Stratford, W., Seward, A., Henderson, M., Savage, M. K., Smith, E., et al. (2010). Crust–mantle structure of the central North Island, New Zealand, based on seismological observations. *Journal of Volcanology and Geothermal Research*, 190(1–2), 58–74. <https://doi.org/10.1016/J.JVOLGEORES.2009.11.017>
- Suzuki, K., Nakano, M., Takahashi, N., Hori, T., Kamiya, S., Araki, E., et al. (2016). Synchronous changes in the seismicity rate and ocean-bottom hydrostatic pressures along the Nankai trough: A possible slow slip event detected by the Dense Oceanfloor Network system for Earthquakes and Tsunamis (DONET). *Tectonophysics*, 680, 90–98. <https://doi.org/10.1016/j.tecto.2016.05.012>
- Thompson, G., & Reyes, C. (2017). GISMO—A seismic data analysis toolbox for MATLAB [software].
- Todd, E. K., & Schwartz, S. Y. (2016). Tectonic tremor along the northern Hikurangi Margin, New Zealand, between 2010 and 2015. *Journal of Geophysical Research: Solid Earth*, 121, 8706–8719. <https://doi.org/10.1002/2016JB013480>
- Todd, E. K., Schwartz, S. Y., Mochizuki, K., Wallace, L. M., Sheehan, A. F., Webb, S. C., et al. (2018). Earthquakes and tremor linked to seamount subduction during shallow slow slip at the Hikurangi Margin, New Zealand. *Journal of Geophysical Research: Solid Earth*, 123, 6769–6783. <https://doi.org/10.1029/2018JB016136>
- Uchida, N., Iinuma, T., Nadeau, R. M., Bürgmann, R., & Hino, R. (2016). Periodic slow slip triggers megathrust zone earthquakes in northeastern Japan. *Science (New York, N.Y.)*, 351(6272), 488–492. <https://doi.org/10.1126/science.aad3108>
- Vallée, M., Nocquet, J.-M., Battaglia, J., Font, Y., Segovia, M., Régnier, M., et al. (2013). Intense interface seismicity triggered by a shallow slow slip event in the Central Ecuador subduction zone. *Journal of Geophysical Research: Solid Earth*, 118, 2965–2981. <https://doi.org/10.1002/jgrb.50216>
- Wallace, L. M., Barnes, P., Beavan, J., Van Dissen, R., Litchfield, N., Mountjoy, J., et al. (2012). The kinematics of a transition from subduction to strike-slip: An example from the central New Zealand plate boundary. *Journal of Geophysical Research*, 117, B02405. <https://doi.org/10.1029/2011JB008640>
- Wallace, L. M., & Beavan, J. (2010). Diverse slow slip behavior at the Hikurangi subduction margin, New Zealand. *Journal of Geophysical Research*, 115, B12402. <https://doi.org/10.1029/2010JB007717>

- Wallace, L. M., Beavan, J., Bannister, S. C., & Williams, C. (2012). Simultaneous long-term and short-term slow slip events at the Hikurangi subduction margin, New Zealand: Implications for processes that control slow slip event occurrence, duration, and migration. *Journal of Geophysical Research*, 117, B11402. <https://doi.org/10.1029/2012JB009489>
- Wallace, L. M., Beavan, J., McCaffrey, R., & Desmond, D. (2004). Subduction zone coupling and tectonic block rotations in the North Island, New Zealand. *Journal of Geophysical Research*, 109, B12406. <https://doi.org/10.1029/2004JB003241>
- Wallace, L. M., & Eberhart-Phillips, D. (2013). Newly observed, deep slow slip events at the central Hikurangi margin, New Zealand: Implications for downdip variability of slow slip and tremor, and relationship to seismic structure. *Geophysical Research Letters*, 40, 5393–5398. <https://doi.org/10.1002/2013GL057682>
- Wallace, L. M., Hreinsdóttir, S., Ellis, S., Hamling, I., D'Anastasio, E., & Denys, P. (2018). Triggered slow slip and afterslip on the Southern Hikurangi subduction zone following the Kaikōura earthquake. *Geophysical Research Letters*, 45, 4710–4718. <https://doi.org/10.1002/2018GL077385>
- Wallace, L. M., Kaneko, Y., Hreinsdóttir, S., Hamling, I., Peng, Z., Bartlow, N. M., et al. (2017). Large-scale dynamic triggering of shallow slow slip enhanced by overlying sedimentary wedge. *Nature Geoscience*, 10(10), 765–770. <https://doi.org/10.1038/ngeo3021>
- Wallace, L. M., Reyners, M., Cochran, U., Bannister, S. C., Barnes, P. M., Berryman, K. R., et al. (2009). Characterizing the seismogenic zone of a major plate boundary subduction thrust: Hikurangi Margin, New Zealand. *Geochemistry, Geophysics, Geosystems*, 10, Q10006. <https://doi.org/10.1029/2009GC0002610>
- Wallace, L. M., Webb, S. C., Ito, Y., Mochizuki, K., Hino, R., Henrys, S., et al. (2016). Slow slip near the trench at the Hikurangi subduction zone, New Zealand. *Science*, 352(6286), 701–704. <https://doi.org/10.1126/science.aaf2349>
- Warren-Smith, E., Fry, B., Kaneko, Y., & Chamberlain, C. J. (2018). Foreshocks and delayed triggering of the 2016 M_W 7.1 Te Araroa earthquake and dynamic reinvigoration of its aftershock sequence by the M_W 7.8 Kaikōura earthquake, New Zealand. *Earth and Planetary Science Letters*, 482, 265–276. <https://doi.org/10.1016/j.epsl.2017.11.020>
- Warren-Smith, E., Fry, B., Chon, E. R., Henrys, S. A., Sheehan, A. F., Mochizuki, K., & Schwartz, S. Y. (2018). Episodic stress tensor and fluid pressure cycling in subducting oceanic crust during Northern Hikurangi slow slip events (invited). In *American Geophysical Union, Fall Meeting 2018*, abstract id. T53C-03.
- Webb, T. H., & Anderson, H. (1998). Focal mechanisms of large earthquakes in the North Island of New Zealand: Slip partitioning at an oblique active margin. *Geophysical Journal International*, 134(1), 40–86. <https://doi.org/10.1046/j.1365-246x.1998.00531.x>
- Wiemer, S., & Wyss, M. (2000). Minimum magnitude of completeness in earthquake catalogs: Examples from Alaska, the Western United States, and Japan. *Bulletin of the Seismological Society of America*, 90(4), 859–869. <https://doi.org/10.1785/0119990114>
- Williams, C. A., Eberhart-Phillips, D., Bannister, S. C., Barker, D. H. N., Henrys, S. A., Reyners, M., & Sutherland, R. (2013). Revised interface geometry for the Hikurangi Subduction Zone, New Zealand. *Seismological Research Letters*, 84(6), 1066–1073. <https://doi.org/10.1785/0220130035>
- Woessner, J., & Wiemer, S. (2005). Assessing the quality of earthquake catalogues: Estimating the magnitude of completeness and its uncertainty. *Bulletin of the Seismological Society of America*, 95(2), 684–698. <https://doi.org/10.1785/0120040007>